VILNIUS TECH
Vilnius Gediminas Technical University

AVIATION
ISSN: 1648-7788 / eISSN: 1822-4180
2022 Volume 26 Issue 2: 79–88
https://doi.org/10.3846/aviation.2022.16878

COMPARING FUEL-OPTIMAL AND SHORTEST PATHS WITH OBSTACLE AVOIDANCE

Ibrahim H. CIHAN *#

Department of Mechanical & Aerospace Engineering, University of Missouri, Columbia, USA

Received 13 March 2021; accepted 18 August 2021

Abstract. This paper presents a comparison of fuel-optimal and shortest paths of an unmanned combat aerial vehicle (UCAV) with obstacle avoidance. A nonlinear constrained optimization algorithm is applied to obtain the optimal paths. An initial value problem (IVP) and an inverse-dynamics approach are used separately to determine optimal paths for various scenarios and in order to reduce computation time. While inputs of the optimization algorithm are discrete control variables in the IVP method, discrete state variables are used as inputs in the inverse-dynamics method. The minimized path segments of the geometrical model provide an initial estimation of the heading angle for the aircraft flight mechanics model. The number of variables used by the optimization algorithm has a direct effect upon the optimal accuracy; however, the computation time is inversely proportional to the number of the variables. Simulation results demonstrate that the proposed IVP method effectively converges to optimal solutions.

Keywords: fuel-optimal path, shortest path, geometric approach, initial value problem, inverse dynamics, fmincon, obstacle avoidance.

Introduction

Unmanned Aerial Vehicles (UAVs) can be controlled autonomously by an operator outside of the vehicle or via an onboard computer. UAV designs are based upon mission parameters and their objectives. These categories include size, user, and mission purpose (Force, 2011; Hanscom & Bedford, 2013). The largest military aircraft in this study, the X-47A, is used mainly for intelligence, surveillance, and reconnaissance (ISR) mission purposes. The primary objective of the X-47A is to perform ISR at cruising altitude by avoiding obstacles, which are radars placed on aerial maps. It is assumed that the locations and detection ranges of radars are known in advance. Fuel efficiency directly impacts the range of an aircraft; hence, fuel consumption should be minimized to increase range. Several parameters affect the fuel efficiency of an aircraft. Some of these parameters (including engine types and number, aspect ratio, wing area, empty weight, etc.) are constant during flight. Conversely, other parameters (including operating altitude, throttle, flight speed, lift-to-drag ratio (L/D), etc.) can be set during the flight in order to reduce fuel consumption. Therefore, path optimization techniques are essential to determine the optimum parameters and the best performance.

Path planning is one of the most popular subtopics in UAV applications. Different methods and software packages have been developing for solving path-planning problems. The Mixed Integer Linear Programming (MILP) method was applied to obtain optimal trajectories for single or multiple vehicles (Albert et al., 2017; Cafieri & Durand, 2014; Chen et al., 2020; Richards & How, 2002; Schouwenaars et al., 2001; Zhang et al., 2014). The dynamic model was changed into a linearized form by using MILP with discrete states and controls. Schouwenaar et al. (2001) investigated the fuel-optimal trajectory for multiple vehicles to determine ideal obstacle avoidance. The authors utilized the CPLEX and A Mathematical Programming Language (AMPL) optimization algorithm. Richards and How (2002) used the MILP method to minimize fuel consumption and flight time in two separate scenarios. The authors replaced circular obstacle constraints with square and polygon obstacles to convert nonlinear constraints to linear constraints. Chen et al. (2020) presented the MILP and improved A-star algorithms for UAV path planning problems in order to improve the node selection strategy and to effectively achieve the optimal path. The major drawback of the MILP method is the restriction to linear problems.

*Corresponding author. E-mail: *ihc7w6@mail.missouri.edu*

#Faculty of Aerospace Sciences, Aerospace Engineering, Tarsus University, Tarsus, Turkey

Bortoff (2000) developed a two-step path planning algorithm for UAVs to minimize the total ground-track length. In the first step, a Voronoi diagram with discrete vertices and edges was created. Next, the virtual-forces approach was implemented using the Voronoi diagram's solution as an initial guess.

The cruise is the longest part of the flight. Ardema and Asuncion (2009), Fan et al. (2020), Jensen et al. (2015), and Turgut et al. (2014) present cruise-flight optimization studies to reduce the fuel consumption of commercial aircraft. Ardema and Asuncion (2009) compared the results of a singular optimal control problem and the Brequet range equation (for constant altitude and velocity). Green's theorem was used to solve the singular optimal control problem. Fan et al. (2020) developed a new optimization algorithm for cruise flight trajectory where optimal cruise speed is parameterized by a linear function of altitude to reduce the operating cost of a flight.

Hybrid propulsion system is one of the promising technologies as it contributes to environmental sustainability. The reduction in energy consumption results in a decrease in environmental pollution (Tian et al., 2019). To reduce energy consumption, Bai et al. (2020) and Dobrokhodov et al. (2020) recently presented energy-optimal guidance algorithms for hybrid UAVs.

A Direct Collocation with Nonlinear Programming (DCNLP) method was utilized to solve optimal control problems (Geiger et al., 2006). First, cubic polynomial functions approximated the trajectories between state and control nodes. Second, the optimal control problem was converted to a nonlinear programming problem. Lastly, MATLAB's fmincon solver was used to obtain the optimum state and control values. Liu et al. (2012) used the Gauss pseudospectral method (GPM) to find the optimal solution for reconnaissance missions of stealth UAVs. The authors investigated minimum fuel consumption, minimum flight time, and minimum probability of detection in separate cases. To solve optimal control problems in Mohan et al. (2012), the pseudospectral method and a rapidly exploring random tree (RRT) algorithm were utilized. The RRT algorithm (Ferguson & Stentz, 2006; Mohan et al., 2012; Tsai et al., 2015; Véras et al., 2019; Zammit & Van Kampen, 2018), which seeks the shortest path between two coordinates, provided initial guesses for the optimal control problems. Tsai et al. (2015) employed the RRT and A-star algorithms to determine a low-cost flight path for multirotor aerial vehicles. Call (2006) assessed the RRT and genetic algorithms to compare their convergence properties and computation times in the pre-mission path planning phase. The RRT algorithm gained an advantage over the genetic algorithm for computation time, whereas the genetic algorithm determined a better path with convergence towards a solution. Macharet et al. (2010), Shima et al. (2005), Sonmez et al. (2015), and Wang and Chen (2014), also present various genetic algorithms for UAV path designs. Wang and Chen (2014) developed a new method to improve the traditional genetic algorithm by reducing computation time.

The primary goal of this study is to find fuel-optimal and shortest paths in a level flight at 9,144 m (30,000 ft) for two different scenarios (one-way path with one destination point and closed path with three destination points) and to make a comparison between them. The secondary goal is to reduce the computation time of the optimization algorithm. To achieve these two objectives, the IVP and the inverse-dynamics methods were implemented in MATLAB's fmincon algorithm. Inputs of the optimization problems are discrete control variables (throttle and bank angle) in the IVP method while discrete state variables (velocity, heading angle, and mass of the aircraft) are used as inputs in the inverse-dynamics method. Simulation scenarios are run for the flight mechanics model with 10–50 discrete stages on the path. This study differs from the previous work on path optimization methods by developing a geometric short-path approach for the flight mechanics model in order to improve convergence to the optimal paths. Simulation results demonstrate that the use of the geometric model in the inverse-dynamics method is a key factor in quickly and effectively achieving the optimization results for the flight mechanics model.

1. System model

1.1. Aircraft description

The Northrop Grumman X-47A Pegasus is used as the UCAV model for optimization problems. The aircraft was produced by Boeing and Northrop Grumman as the first variant of the X-47 series. General specifications of the X-47A are presented in detail in Cihan (2016). Oswald efficiency (e) and zero-lift drag coefficient (C_{D0}) are not available because of its classified nature. X-47A is a tailless delta-wing aircraft. Typical values of Oswald efficiency and zero-lift drag coefficient for subsonic delta-wing jets are in the range of 0.70–0.75 and 0.009–0.014, respectively. After some preliminary calculations were performed using the data in Brandt et al. (2004), Cihan (2016), Sadraey and Müller (2009), these aerodynamic properties are set as $C_{D0} = 0.011$ and $e = 0.75$, which satisfy the published specifications for range of 2,778 km (1500 nmi), service ceiling of 12,192 m (40,000 ft), and maximum speed (high subsonic).

1.2. Propulsion system

The X-47A is powered by a Pratt & Whitney Canada JT15D-5C engine. It is a low bypass ratio turbofan engine with thrust = 14,190 N (3,190 lbf) at takeoff. Detailed information about the engine specification can be found in Cihan (2016). Using MATLAB, a function was created for calculating thrust (T) and thrust specific fuel consumption (TSFC or c_t) given altitude (h) and velocity (V) as inputs. Fuel mass-flow rate can be computed from thrust and TSFC:

$$\dot{m}_{\text{fuel}} = -c_t T. \tag{1}$$

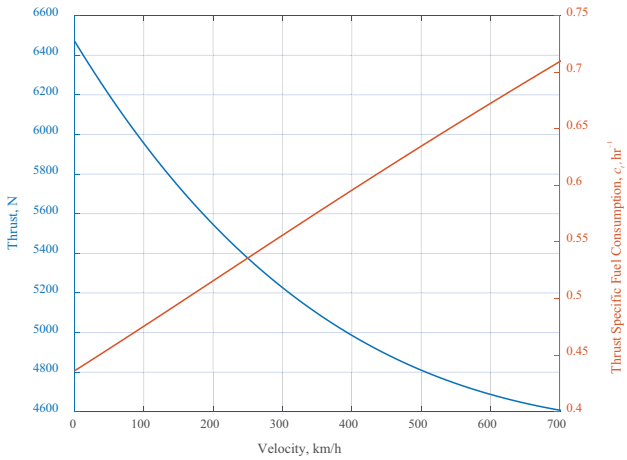

Figure 1. Thrust and TSFC vs. velocity at 9,144 m

Figure 1 presents maximum thrust available and TSFC vs. velocity profiles at 9,144 m (30,000 ft) for Pratt & Whitney Canada JT15D-5C engine. Figure 1 shows that the thrust (blue curve) and TSFC (orange curve) approximately follow exponential decay and linear growth profiles with velocity, respectively. The fuel efficiency of a low-speed flight is better than a high-speed flight; on the other side, thrust decreases with velocity, as seen in Figure 1. Therefore, velocity should be optimized in order to minimize the fuel mass-flow rate in Eq. (1) for the fuel-optimal path planning problem.

1.3. Obstacle avoidance

Primary surveillance radars (PSRs) are used as obstacles in this study. The maximum detectable range of radar can be calculated with the radar cross section (RCS) of an aircraft and specifications of the radar system; see Cihan (2016) for detailed information. PSRs scan circular areas on aerial maps, so circular obstacles are used to define inequality constraints in the optimization problems.

2. Optimization

Fmincon is a nonlinear programming solver in MATLAB. The fmincon algorithm searches the design space for the minimum value of a constrained nonlinear multivariable function. In the optimization problem, initial guesses for variables should be chosen wisely so that convergence to the optimum values occurs quickly.

2.1. Problem definition

The goal of the optimization problem is to separately achieve the fuel-optimal path (case 1) and shortest path (case 2). For case 1, the integration of the mass-flow rate is used as a cost function in Eq. (2a) to determine minimum fuel consumption in the optimization problem while the integration of velocity is defined by Eq. (2b) as a cost function for case 2 to provide distance s along the flight path. The problem statement is

Minimize:

$$F_1(x) = \int_{t_0}^{t_f} \dot{m}_{\text{fuel}}\, dt = \int_{t_0}^{t_f} -c_t T dt; \tag{2a}$$

$$F_2(x) = \int_{t_0}^{t_f} \dot{s} dt = \int_{t_0}^{t_f} V dt. \tag{2b}$$

Subject to:

$$\begin{cases} \dot{y}_1 = \dot{X} = V\cos\Psi, & X(0) = 0 \Rightarrow \text{fixed} \\ \dot{y}_2 = \dot{Y} = V\sin\Psi, & Y(0) = 0 \Rightarrow \text{fixed} \\ \dot{y}_3 = \dot{V} = \dfrac{T - D}{m}, & V(0) = V_0 \Rightarrow \text{free} \\ \dot{y}_4 = \dot{\Psi} = \dfrac{L\sin\Phi}{mV}, & \Psi(0) = \Psi_0 \Rightarrow \text{free} \\ \dot{y}_5 = \dot{m} = -c_t T, & m(0) = m_0 \Rightarrow \text{fixed} \end{cases}, \tag{3}$$

where V is the velocity, Ψ is the heading angle, D is the drag force, L is the lift force, and Φ is the bank angle. State differential equations (SDEs) in Eq. (3) are the horizontal velocities in the direction of X and Y axes, acceleration, heading rate, and mass-flow rate, respectively. Initial conditions for mass and position coordinates are known and fixed. On the other hand, the initial velocity and initial heading angle of the aircraft are free. The constraints for both optimization problems (case 1 and case 2) are

$$\begin{cases} c_{\text{eq}}(1) = X(t_f) - X_{\text{target}} = 0 \\ c_{\text{eq}}(2) = Y(t_f) - Y_{\text{target}} = 0 \end{cases}; \tag{4}$$

$$c_i = \sqrt{\left(X(t) - X_{i,\text{radar}}\right)^2 + \left(Y(t) - Y_{i,\text{radar}}\right)^2} > r_{i,\text{radar}}^2. \tag{5}$$

Equality constraints in Eq. (4) show that the aircraft's coordinates must match the target's coordinates at the end of the cruise. The aircraft must also be outside of the circular radar detection range during the cruise for inequality equations in Eq. (5) to be satisfied. Inverse dynamics and IVP methods are applied in optimization problems.

2.2. Method 1 – Initial Value Problem (IVP)

The MATLAB function ode45 is used to integrate the SDEs. Control variables throttle (δ) and bank angle (Φ) are the inputs to the dynamic system. Each control variable has N discrete values along the trajectory. In addition, scaling factors, a_{velocity}, $a_{\text{heading\_angle}}$, and $a_{\text{flight\_time}}$, are used as optimization variables to determine the free-flight time (t_{flight}), initial velocity (V_{initial}), and initial heading angle (Ψ_{initial}). Hence, the total number of variables is $N(\delta) + N(\Phi) + a_{\text{velocity}} + a_{\text{heading\_angle}} + a_{\text{flight\_time}} = 2N+3$. In the optimization problems, lower and upper bounds are set for the two control variables. Throttle varies between zero and one, which corresponds to 100% throttle and maximum engine thrust at a given velocity and altitude. The lower and upper bounds for bank angle depend on

the weight of the aircraft W, maximum lift-over-drag ratio $(L/D)_{\max}$, and maximum thrust available $T_{\max}$:

$$\Phi_{\max} = \cos^{-1}\left(\frac{W}{(L/D)_{\max} T_{\max}}\right). \quad (6)$$

Positive and negative signs for bank angle indicate left and right turns, respectively.

2.3. Method 2 – inverse dynamics

Discrete state variables velocity V, heading angle Ψ, and mass m are used as the inputs for an inverse-dynamics approach to solve the SDEs. Then, the control variables throttle (δ) and bank angle (Φ) can be computed from state rates in Eq. (3) and the balance of forces normal to the level flight path:

$$L\cos\Phi = W = mg. \quad (7)$$

The bank angle (Φ) equation is derived from Eq. (7) and the fourth SDE in Eq. (3):

$$\dot{\Psi} = \frac{L\sin\Phi}{mV} = \frac{(mg/\cos\Phi)\sin\Phi}{mV} \Rightarrow \Phi = \tan^{-1}\left(\frac{\dot{\Psi}V}{g}\right). \quad (8)$$

To compute the kinetic equations $\dot{X}$ and $\dot{Y}$, N discrete values are defined for velocity and heading angle along the trajectory. Linear segments connect the discrete values. The cumulative trapezoidal numerical integration method (cumtrapz) in MATLAB is applied to integrate the kinematic equations. The cumtrapz method determines the area under the velocity component curves to obtain the position coordinates. The slopes of the segments on the velocity and heading-angle curves represent acceleration $\dot{V}$ and heading rate $\dot{\Psi}$, respectively. To calculate the fifth SDE (mass-flow rate), the thrust required is computed using the third SDE with the mass of the aircraft, acceleration, and drag at each discrete stage:

$$\dot{V} = \frac{\Delta V}{\Delta t} = \frac{V_{i+1} - V_i}{\Delta t} = \frac{T - D}{m} \Rightarrow T = m\frac{\Delta V}{\Delta t} + D, \quad (9)$$

where Δt is the elapsed time between two discrete stages, which can be found by dividing the total flight time by the number of linear segments:

$$\Delta t = \frac{t_{\text{flight}}}{N-1}. \quad (10)$$

At the first discrete stage, the mass of the aircraft is known and fixed, so there are N-1 discrete values and N-1 equality constraints for the mass variable:

$$\begin{aligned} m_2 &= m_1 - \dot{m}_{\text{fuel}\_1}\Delta t \\ m_3 &= m_2 - \dot{m}_{\text{fuel}\_2}\Delta t \\ &\vdots \quad \vdots \quad \vdots \\ m_N &= m_{N-1} - \dot{m}_{\text{fuel}_{N-1}}\Delta t \end{aligned} \quad . \quad (11)$$

In the inverse-dynamics method, only the flight-time scaling factor $a_{\text{flight\_time}}$ is considered as an optimization variable because initial velocity and initial heading angle are defined by N discrete values. The total number of variables is $N(V) + N(\Psi) + N\text{-}1(m) + a_{\text{flight\_time}} = 3N$.

The procedure for finding an optimal path by avoiding obstacles differs from the procedure of the optimal path-planning without obstacles. Our optimal-path design by avoiding obstacles follows a three-step process: 1) computing the shortest path that avoids the static obstacles in a horizontal plane without regard for flight mechanics, 2) utilizing a geometric approach that simplifies the shortest path into linear segments without regard for flight mechanics, and 3) solving flight mechanics optimization problems.

Figure 2 shows a simple simulation environment where three circular obstacles are added between point A and point B. The M-file shpath (Cihan, 2016; Kleder, 2008) is performed to determine the shortest path from point A to point B while avoiding obstacles. The inputs of the M-file are a grid matrix (zeros (blue area in Figure 2) represent safe area and ones (red area in Figure 2) represent obstacles), initial coordinates (X_i, Y_i), and destination coordinates (X_f, Y_f). The M-file searches the X and Y waypoints of the path by tracking zeros on the grid matrix. For the first step, the shortest path is determined as the green curve in Figure 2.

In the second step, a geometric approach is applied to provide a good estimate for N discrete heading-angle variables. N+1 stages are chosen from the shortest path in Figure 3 in order to have N linear segments and N slopes of these segments. Each slope is used to estimate the heading-angle variables for the flight mechanics model:

$$\frac{\Delta Y}{\Delta X} = \frac{Y_{i+1} - Y_i}{X_{i+1} - X_i} \equiv \tan\Psi_i, \quad (12)$$

where X and Y are the discrete values without regard for flight mechanics equations of motion. The total length of the N segments is minimized in the Fmincon optimization algorithm:

Minimize:

$$F(x) = \sum_{i=1}^{N}\sqrt{(X_{i+1} - X_i)^2 + (Y_{i+1} - Y_i)^2}. \quad (13)$$

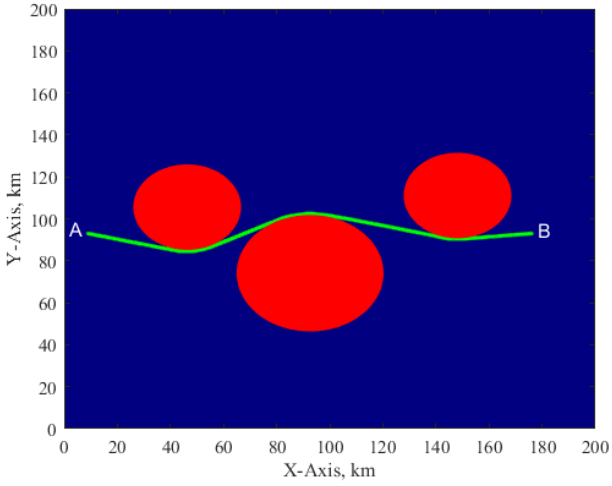

Figure 2. Shortest path for a sample obstacle-avoidance simulation environment without regard for flight mechanics

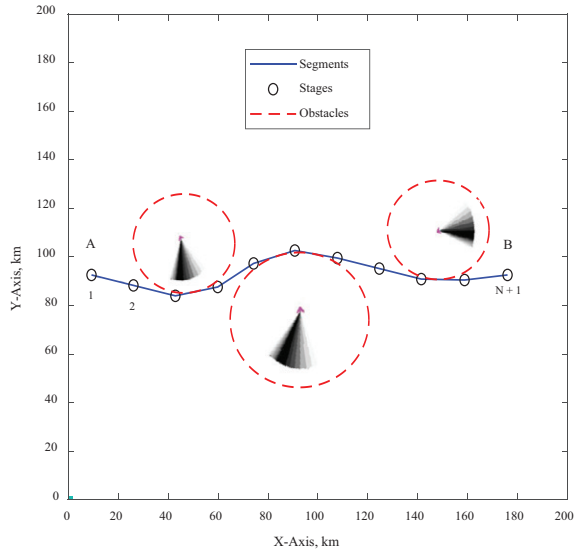

Figure 3. Geometric model for a sample obstacle-avoidance simulation environment without regard for flight mechanics

N-1 equality constraints were used in the geometric-optimization problem so that the length of each segment is equal in order to improve the accuracy of the flight mechanics model. Furthermore, inequality constraints in Eq. (5) are considered in the geometric approach in order to avoid the circular radar.

3. Numerical results

3.1. Optimal paths without obstacles

In the absence of obstacles, the minimum-fuel path can be achieved by following the shortest (straight-line) path between two specified coordinates. IVP (method 1) and inverse dynamics (method 2) are executed to attain a minimum-fuel path without obstacle avoidance for the straight, level flight at 9,144 m (30,000 ft). The initial coordinates of the cruise are set to (0, 0), and the destination point is (1296.4, 1296.4) km, which is equivalent to (700, 700) nmi. Ten discrete stages are taken on the straight-line path for method 1 with 23 variables and method 2 with 30 variables. Note that after comparing the fuel consumption results in Cihan (2016) for variable-cruise altitude and constant-cruise altitude, it was found that constant-cruise altitude is more fuel-efficient. Hence, cruise altitude remains constant at 9,144 m (30,000 ft) for the optimization problems in this paper.

In the first method, V_{initial} = 467.61 km/h, Ψ_{initial} = 45 deg, and t_{flight} = 14,340 sec was computed using the ode45 and Fmincon solvers. The optimal throttle is between 0.651 and 0.381 during the cruise. Bank angle remains zero deg because the aircraft flies with an expected 45 deg heading angle during cruise due to the lack of obstacles.

In the second method, the optimal velocity continually decreases from 521.58 km/h to 400.51 km/h with 14,497 sec of flight time. The optimal bank angle (0 deg) and heading angle (45 deg) are the same as method 1. The mass of the aircraft is 2,390.48 kg (163.8 slugs) at the initial for both methods and decreases with time due to fuel consumption. Table 1 compares the numerical solutions for methods 1 and 2. The fuel efficiency of the inverse-dynamics method is slightly better than the IVP method. Although the IVP has fewer optimization variables, the inverse-dynamics method solves the optimization problem approximately four times faster (note that the computer used for analyses in this work has the following system specifications: Intel® Core™ i5-3230M CPU @ 2.67GHz and 4 GB RAM). Consequently, the inverse-dynamics method is only used for the remainder of the optimization problems.

Table 1. Optimization results of initial value problem and inverse dynamics methods

Method	Number of optimization variables	Computation time (sec)	Minimized fuel consumption (kg)	Total Range (km)
Initial value problem	23	70.0	545.52	1,833.4
Inverse dynamics	30	16.8	542.46	1,833.4

3.2. Optimal paths with obstacle avoidance

In this section, the fuel and shortest-path optimization problems are examined under two different obstacle avoidance scenarios: "one-way path with one destination point" and "closed path with three destination points."

3.2.1. Scenario 1 – one-way path with one destination point

The objective of this scenario is to compare the fuel-optimal and shortest-path cases for one destination mission in an obstacle-rich simulation environment. Before starting to solve flight mechanics optimization problems, the shortest path and geometric approach steps were implemented as described in section 3. Figure 4 presents the simulation

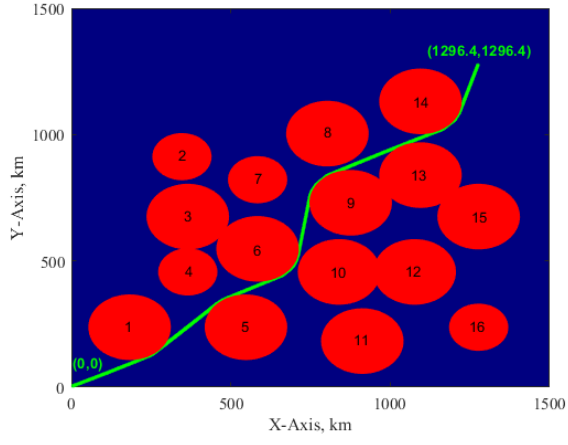

Figure 4. Shortest path by avoiding 16 radars without regard for flight mechanics for scenario 1

environment for the first scenario with sixteen radars. The small radars (radar numbers 2, 4, 7, and 16) scan circles with 92.6 km (50 nmi) radius, and the detection ranges of the rest of the radars are 129.64 km (70 nmi). The green curve in Figure 4 shows the shortest path between the initial point (0, 0) and target point (1296.4, 1296.4) km (recall that the green curve in Figure 4 is achieved using the M-file shpath without regard for flight mechanics).

After the shortest path was determined, 11 discrete stages were selected from the shortest path for the geometric approach to achieve 10 linear segments. Ten optimal segments and slopes are attained by minimizing the total length from Eq. (13). Figure 5 shows the geometric model solution for the first scenario with 10 stages. Each segment slope implies an initial guess of the heading angle from Eq. (12) for the flight mechanics model. The total length of the 10 segments is 2,008.7 km.

Finally, the fuel and shortest-path optimization problems can be solved for flight mechanics using reasonable 10 velocity (it is assumed that the initial estimation of velocity is V_i = 450 km/h at each discrete state), 9 mass (the trend between mass and stage number is nearly linear, so the initial mass stages are estimated by a decreasing linear function with a slope function of 70 kg), and one flight-time scaling (16,000 sec) variables with 10 heading-angle variables found from geometrical path segments. These 30 initial guesses are the initial point of the Fmincon optimization solver to minimize the fuel consumption and range into two separate cases. Figure 6 shows the fuel-optimal and shortest-path optimization results for the first scenario with 10 stages. The blue and magenta curves in Figure 6 represent, respectively, the fuel-optimal and shortest paths by avoiding 16 PSRs. The aircraft successfully completes the ISR mission in a level flight at 9,144 m for the fuel-optimal path with 591.2 kg of fuel consumption and 1,967.9 km of total range while for the shortest path with 624.9 kg of fuel consumption and 1,958.5 km of total range (9.4 km less than the total range of the fuel-optimal path). Although the total range values of fuel-optimal and shortest-path cases are close to each other, the optimal velocity profiles cause a difference in fuel consumption between fuel-optimal and shortest-path cases due to having different optimal-velocity profiles.

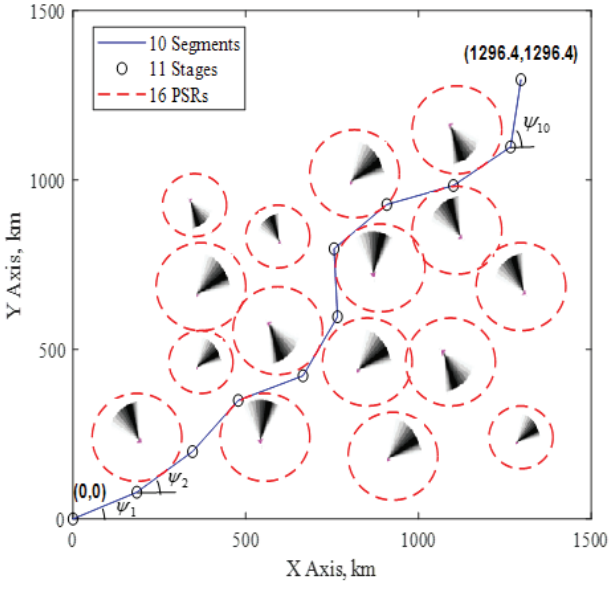

Figure 5. Geometric model without regard for flight mechanics for scenario 1

Table 2 presents the optimized slopes from the minimized-path segments for the geometric model solution and optimal heading angles from the minimized-fuel (case 1) and minimized-range (case 2) paths for the flight mechanics model. For both cases, optimal heading angles at each stage follow the trend of the optimized slopes from the geometric minimum-length optimization. This demonstrates that the geometric model provides a good prediction for the flight mechanics of the optimization problem.

Four additional fuel-optimal and shortest paths were determined for stage numbers with 20, 30, 40, and 50. Table 3 presents the simulation results of each case for

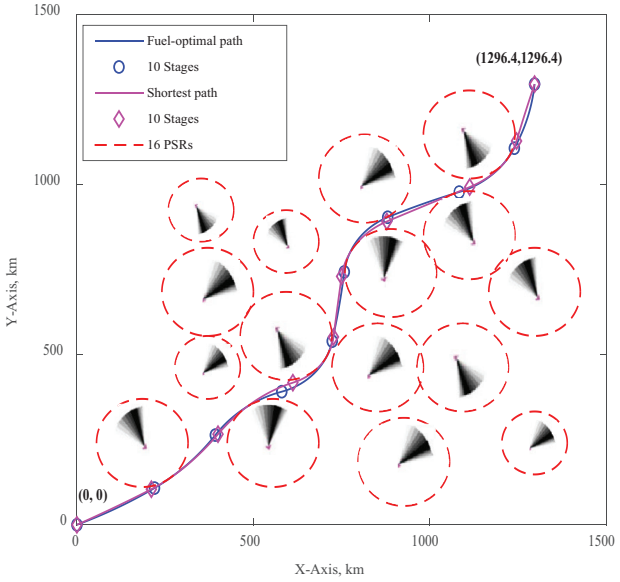

Figure 6. Ten-stage optimal path comparison in scenario 1

Table 2. Optimization results of heading angle for geometric and flight mechanics models

Segment number	Optimal slope for geometric model (deg)	Optimal heading angle for case 1 (deg)	Optimal heading angle for case 2 (deg)
1	23.2	21.1	24.9
2	36.5	31.5	28.2
3	48.9	52.7	50.7
4	21.1	15.3	17.7
5	60.3	77.9	82.8
6	92.8	82.9	82.4
7	40.5	22.8	23.5
8	16.2	17.3	23.2
9	34.5	62.1	74.2
10	81.5	84.4	72.0

fuel consumption and total range. As the number of stages on the path increases, the fuel consumption and total range decrease due to the extra degrees of freedom. Table 3 shows that a higher number of stages offers little performance gain in fuel consumption and total flight range between the desired initial and target coordinates. On the other hand, the Fmincon solver requires a higher computational cost to solve the optimization problem with a large number of discrete state variables.

Figure 7 shows velocity time histories for the fuel and shortest-path cases with 10 and 50 stages at 9,144 m (30,000 ft). Four optimized velocity profiles in Figure 7 are in a decreasing trend over time. Initial optimal velocity values for 50-stage cases are about 20–25% higher than for 10-stage cases. Figure 7 shows that the optimal velocity values in simulations other than case 2 with 10 stages are typically between 400 and 500 km/h while the velocity profile for case 2 with 10 stages has a wide range in order to intend to achieve the shortest path with smaller degrees of freedom. The total flight times for the four trials in Figure 7 are between 15,605 and 16,575 sec.

Table 3. Comparison of fuel and shortest-path optimization results for scenario 1

Method	Number of stages	Number of variables	Fuel consumption (kg)	Total range (km)
Fuel-optimal paths	10	30	591.2	1,967.9
	20	60	586.4	1,957.0
	30	90	585.1	1,956.3
	40	120	584.4	1,955.3
	50	150	583.9	1,955.0
Shortest paths	10	30	624.9	1,958.5
	20	60	600.9	1,952.4
	30	90	596.6	1,951.1
	40	120	600.2	1,950.7
	50	150	592.6	1,950.5

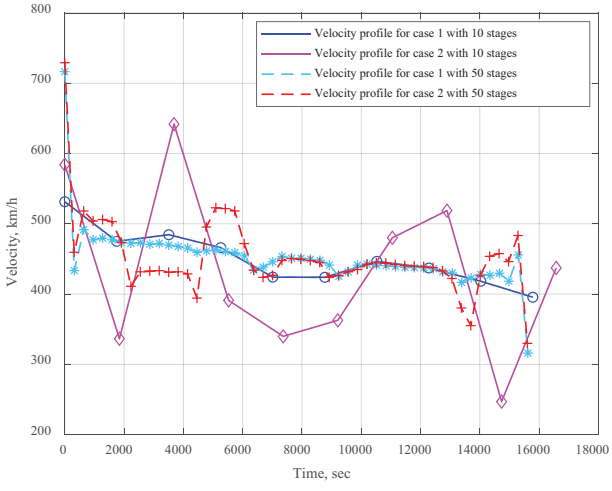

Figure 7. Optimal velocity profiles for four simulations in scenario 1

3.2.2. Scenario 2 – closed-circuit path with three destination points

This scenario aims to compare the fuel and shortest paths by flying over two fixed way-point destination coordinates and avoiding obstacles between starting and final destination coordinates. After the shortest path and the geometric model (recall once again that these two steps are done without regard flight mechanics equations of motion) were determined, the minimized-fuel and minimized-range paths were acquired for the flight mechanics model with 20, 30, 40, and 50 discrete stages on the path in the second scenario (note that a 10-stage case cannot produce usable optimization results for this complex simulation environment). Figure 8 shows the fuel-optimal and shortest paths for 50-stage scenarios. The aircraft starts cruising at point A (0, 0) and flies to the first way-point B. Once the aircraft passes way-point B, it heads towards second way-point C, and then it flies back to starting point A, as shown in Figure 8. Table 4 presents the optimization results of the minimized-fuel and minimized-range cases using 20, 30, 40, and 50 discrete stages in scenario 2. As in the first scenario, increasing the number of discrete stages offers better performance in fuel consumption and total flight range. The fuel efficiency of aircraft in scenario 2 is slightly worse than in scenario 1 because the aircraft requires to perform sharper turns (especially around way-points B and C) in scenario 2 to minimize fuel consumption and total flight range.

Figure 9 shows the optimal velocity histories from the 50-stage fuel and shortest-path optimization results in scenario 2, as well as the stall speed profiles for these two optimization cases. The average optimal velocity range is between 400 and 500 km/h; however, the minimum velocity is observed around way-point C coordinates to make a sharp turning flight about 10,000 sec. At that point, the aircraft's velocity is very close to the stall speed. After way-point C, the aircraft speeds up until it reaches the av-

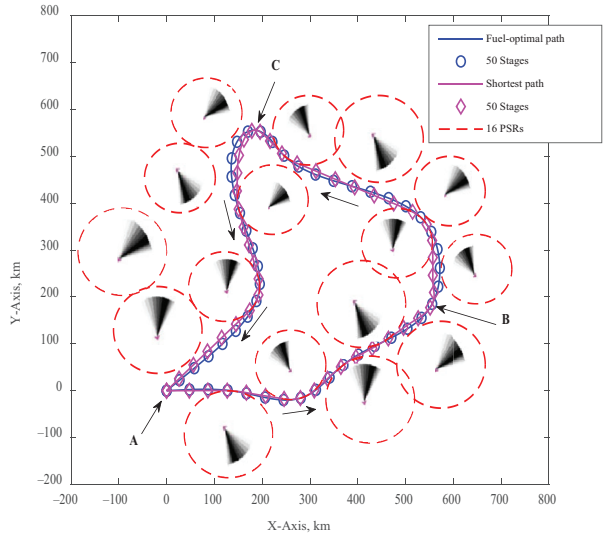

Figure 8. Fifty-stage optimal path comparison in scenario 2

Table 4. Comparison of fuel and shortest-path optimization results for scenario 2

Method	Number of stages	Number of variables	Fuel consumption (kg)	Total range (km)
Fuel-optimal paths	20	60	634.0	1,907.8
	30	90	618.2	1,903.5
	40	120	616.2	1,900.4
	50	150	615.9	1,898.6
Shortest paths	20	60	696.9	1,876.1
	30	90	662.6	1,871.7
	40	120	648.2	1,870.2
	50	150	647.4	1,869.4

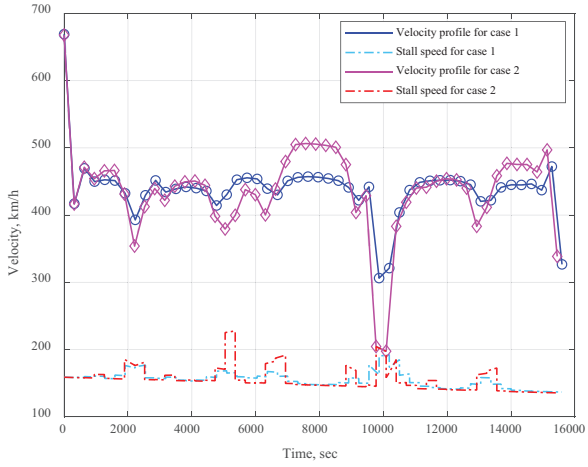

Figure 9. Optimal velocity profiles for two simulations with 50 stages in scenario 2

erage optimal velocity range. The optimal velocity values along the trajectory for both cases are greater than stall speed, which depends on the weight of the aircraft, bank angle, air density, wing area, and maximum lift coefficient. Figure 9 also shows that the stall speed value reaches a peak around 5,000 sec because the aircraft has a higher weight and bank angle at the way-point B when compared to at the way-point C.

Figure 10 presents optimal bank angle profiles from the 50-stage minimized-fuel and minimized-range paths in scenario 2. The larger magnitude of the bank angle takes place around way-point B, about 5,000 sec on the shortest path. The decrease in the weight of the aircraft increases the bank-angle boundary range with time, as seen in Figure 10. Compared to the total flight time, the aircraft can reach the coordinates of its final destination 220 sec earlier by following the shortest-range path.

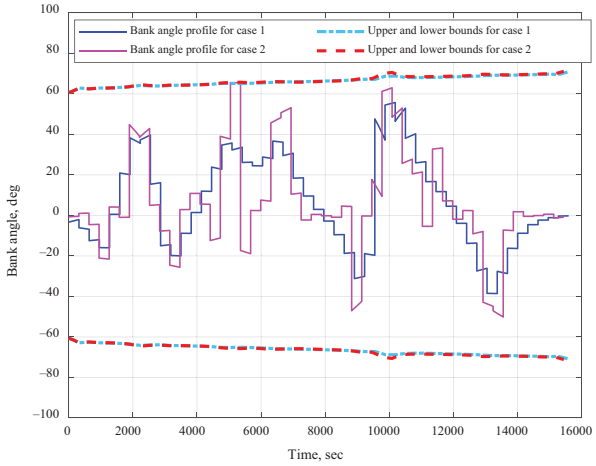

Figure 10. Optimal bank angle profiles for two simulations with 50 stages in scenario 2

Conclusions

In this paper, the fuel and shortest-path optimization problems were investigated, and their results for various scenarios were compared. The state differential equations (SDEs) were solved by initial value problem (IVP, method 1) and inverse dynamics (method 2) approaches. By comparing the two methods for obstacle-free problems, the results indicated that the inverse-dynamics method converged to the solution more rapidly than the IVP method. Therefore, only the inverse-dynamics method was used in the obstacle-rich simulation scenarios: one-way path with one destination point (scenario 1) and closed-circuit path with three destination points (scenario 2). In the second method, a new approach has been developed for both minimized-fuel and minimized-range paths by avoiding obstacles in order to improve convergence to the optimal paths. Firstly, the shortest path was found among the safe areas (without regard for flight mechanics). Then the geometric-optimization problem was applied to estimate initial heading angles at discrete stages (without regard for flight mechanics). Lastly, these initial guesses are used for the flight mechanics of the optimization problem. Initial guesses for the optimization algorithm influenced the accuracy of optimization results and computation time. The geometric short-path model generated a high-quality initial guess for the heading angle profile in the inverse dynamics method. As the number of the discrete stages increased, the fuel efficiency becomes slightly better; however, the increase in computation time is a poor trade-off for beyond a certain higher number of stages. The simulation results showed that the minimized-fuel and minimized-range paths closely follow each other when the simulation environment is not very complex, such as the first scenario. On the other hand, having more complex simulation environments (see the second scenario) resulted in little performance degradation in terms of both fuel efficiency and total flight range due to sharp turning flights.

Funding

This research received no external funding.

References

Albert, A., Leira, F. S., & Imsland, L. S. (2017). UAV path planning using MILP with experiments. *Modelling Identification and Control Journal*, *38*(1), 21–32. https://doi.org/10.4173/mic.2017.1.3

Ardema, M. D., & Asuncion, B. C. (2009). Flight path optimization at constant altitude. In *Variational analysis and aerospace engineering*. Springer. https://doi.org/10.1007/978-0-387-95857-6_2

Bai, M., Yang, W., Song, D., Kosuda, M., Szabo, S., Lipovsky, P., & Kasaei, A. (2020). Research on energy management of hybrid unmanned aerial vehicles to improve energy-saving and emission reduction performance. *International Journal of Environmental Research and Public Health*, *17*(8), 2917. https://doi.org/10.3390/ijerph17082917

Bortoff, S. A. (2000, June 28–30). Path planning for UAVs. In *Proceedings of the 2000 American Control Conference (IEEE Cat. No. CH36334)* (Vol. 1, pp. 364–368). Chicago, IL, USA. https://doi.org/10.1109/ACC.2000.878915

Brandt, S. A., Bertin, J. J., Stiles, R. J., & Whitford, R. (2004). *Introduction to aeronautics: A design perspective*. American Institute of Aeronautics and Astronautics. https://doi.org/10.2514/4.862007

Cafieri, S., & Durand, N. (2014). Aircraft deconfliction with speed regulation: New models from mixed-integer optimization. *Journal of Global Optimization*, *58*(4), 613–629. https://doi.org/10.1007/s10898-013-0070-1

Call, B. R. (2006). *Obstacle avoidance for unmanned air vehicles* [Master thesis, Brigham Young University]. Provo, UT, USA. https://scholarsarchive.byu.edu/cgi/viewcontent.cgi?article=1791&context=etd

Chen, J., Li, M., Yuan, Z., & Gu, Q. (2020, June 12–14). An improved A* algorithm for UAV path planning problems. In 2020 *IEEE 4th Information Technology, Networking, Electronic and Automation Control Conference (ITNEC)* (Vol. 1, pp. 958–962). https://doi.org/10.1109/ITNEC48623.2020.9084806

Cihan, I. H. (2016). *Optimal path planning of an unmanned combat aerial vehicle with obstacle avoidance* [Master thesis, University of Missouri]. Columbia, MO, USA.

Dobrokhodov, V. N., Walton, C., Kaminer, I. I., & Jones, K. D. (2020). Energy-optimal guidance of hybrid ultra-long endurance UAV. *IFAC-PapersOnLine*, *53*(2), 15639–15646. https://doi.org/10.1016/j.ifacol.2020.12.2500

Fan, Y., Yang, L., Li, Q., Nong, C., Zheng, Z., & Xue, F. (2020, June 12–14). Cost index-based cruise flight trajectory optimization. In *2020 IEEE 4th Information Technology, Networking, Electronic and Automation Control Conference (ITNEC)* (Vol. 1, pp. 103–110). IEEE. https://doi.org/10.1109/ITNEC48623.2020.9085146

Ferguson, D., & Stentz, A. (2006, October 9–15). Anytime RRTs. In *Proceedings of the IEEE/RSJ International Conference on Intelligent Robots and Systems* (pp. 5369–5375). Beijing, China. https://doi.org/10.1109/IROS.2006.282100

Force, U. T. (2011). *Unmanned aircraft system airspace integration plan*. Department of Defense.

Geiger, B., Horn, J., DeLullo, A., Niessner, A., & Long, L. (2006, August 21–24). Optimal path planning of UAVs using direct collocation with nonlinear programming. In *AIAA Guidance, Navigation, and Control Conference and Exhibit*. Keystone, CO, USA. American Institute of Aeronautics and Astronautics. https://doi.org/10.2514/6.2006-6199

Hanscom, A. F. B., & Bedford, M. A. (2013). Unmanned aircraft system (UAS) Service Demand 2015–2035. *Literature review & projections of future usage.* Research and Innovative Technology Administration US Department of Transportation, Washington, DC, USA.

Jensen, L., Tran, H., & Hansman, J. R. (2015, June 23–26). Cruise fuel reduction potential from altitude and speed optimization in global airline operations. In *11th USA/Europe Air Traffic Management Research and Development Seminar (ATM2015)* (pp. 497–506). Lisbon, Portugal.

Kleder, M. (2008). *Shortest path with obstacle avoidance (ver 1.3)*. https://www.mathworks.com/matlabcentral/fileexchange/8625-shortest-path-with-obstacle-avoidance-ver-1-3

Liu, H., Chen, S., Shen, L., & Chen, J. (2012). Tactical trajectory planning for stealth unmanned aerial vehicle to win the radar game. *Defence Science Journal*, *62*(6), 375–381. https://doi.org/10.14429/dsj.62.2686

Macharet, D. G., Neto, A. A., & Campos, M. F. M. (2010, October 23–28). Feasible UAV path planning using genetic algorithms and Bézier curves. In *Proceedings of the 20th Brazilian Symposium on Artificial Intelligence* (pp. 223–232). São Bernardo do Campo, Brazil. https://doi.org/10.1007/978-3-642-16138-4_23

Mohan, K., Patterson, M., & Rao, A. (2012, August 13–16). Optimal trajectory and control generation for landing of multiple aircraft in the presence of obstacles. In *AIAA Guidance, Navigation, and Control Conference* (pp. 1–16). Minneapolis, MN, USA. American Institute of Aeronautics and Astronautics. https://doi.org/10.2514/6.2012-4826

Richards, A., & How, J. P. (2002, May 8–10). Aircraft trajectory planning with collision avoidance using mixed integer linear programming. In *Proceedings of the 2002 American Control Conference* (IEEE Cat. No. CH37301) (pp. 1936–1941). Anchorage, AK, USA. IEEE. https://doi.org/10.1109/ACC.2002.1023918

Sadraey, M, & Müller, D. (2009). Drag force and drag coefficient. In *Aircraft performance analysis*. VDM Verlag Dr. Müller.

Schouwenaars, T., De Moor, B., Feron, E., & How, J. (2001, September 4–7). Mixed integer programming for multi-vehicle path planning. In *Proceedings of the 2001 European Control Conference* (pp. 2603–2608). Porto, Portugal. IEEE. https://doi.org/10.23919/ECC.2001.7076321

Shima, T., Rasmussen, S. J., & Sparks, A. G. (2005, March 19–22). UAV cooperative multiple task assignments using genetic algorithms. In *Proceedings of the American Control Conference* (pp. 8–10). Portland, OR, USA. https://doi.org/10.1109/ACC.2005.1470429

Sonmez, A., Kocyigit, E., & Kugu, E. (2015, June 9–12). Optimal path planning for UAVs using genetic algorithm. In *Proceedings of the International Conference on Unmanned Aircraft Systems* (ICUAS) (pp. 50–55). Denver, CO, USA. https://doi.org/10.1109/ICUAS.2015.7152274

Tian, Y., Wan, L., Ye, B., & Xing, D. (2019). Cruise flight performance optimization for minimizing green direct operating cost. *Sustainability*, *11*(14), 3899. https://doi.org/10.3390/su11143899

Tsai, Y. J., Lee, C. S., Lin, C. L., & Huang, C. H. (2015). Development of flight path planning for multirotor aerial vehicles. *Aerospace*, *2*(2), 171–188. https://doi.org/10.3390/aerospace2020171

Turgut, E. T., Cavcar, M., Usanmaz, O., Canarslanlar, A. O., Dogeroglu, T., Armutlu, K., & Yay, O. D. (2014). Fuel flow analysis for the cruise phase of commercial aircraft on domestic routes. *Aerospace Science and Technology, 37*, 1–9. https://doi.org/10.1016/j.ast.2014.04.012

Véras, L. G., Medeiros, F. L., & Guimaraes, L. N. (2019). Rapidly exploring Random Tree* with a sampling method based on Sukharev grids and convex vertices of safety hulls of obstacles. *International Journal of Advanced Robotic Systems*, *16*(1). https://doi.org/10.1177/1729881419825941

Wang, Y., & Chen, W. (2014, July 28). Path planning and obstacle avoidance of unmanned aerial vehicle based on improved genetic algorithms. In *Proceedings of the 33rd Chinese Control Conference* (pp. 8612–8616). Nanjing, China. https://doi.org/10.1109/ChiCC.2014.6896446

Zammit, C., & Van Kampen, E. J. V. (2018, January 8–12). Comparison between A* and RRT algorithms for UAV path planning. In *AIAA Guidance, Navigation, and Control Conference* (pp. 1846–1869). Kissimmee, FL, USA. https://doi.org/10.2514/6.2018-1846

Zhang, L., Zhou, Z., & Zhang, F. M. (2014). Mixed integer linear programming for UAV trajectory planning problem. In *Applied Mechanics and Materials*, *541*, 1473–1477. https://doi.org/10.4028/www.scientific.net/AMM.541-542.1473